



# Numerical modelling of the wave interaction with revetment breakwater built on reclaimed coral reef islands in the South China Sea—Experimental verification

Jianhong Ye<sup>a,\*</sup>, Jipeng Shan<sup>a,d</sup>, Haoran Zhou<sup>a,c</sup>, Naixiao Yan<sup>a,b</sup>

<sup>a</sup> State Key Laboratory of Geomechanics and Geotechnical Engineering, Institute of Rock and Soil Mechanics, Chinese Academy of Sciences, Wuhan, 430071, China

<sup>b</sup> School of Safety Science and Emergence Management, Wuhan University of Technology, Wuhan, 430070, China

<sup>c</sup> University of Chinese Academy of Sciences, Beijing, 100049, China

<sup>d</sup> School of Resources and Environmental Engineering, Wuhan University of Technology, Wuhan, 430070, China

## ARTICLE INFO

### Keywords:

Wave-breakwater interaction  
Revetment breakwater  
Reclaimed calcareous coral sand foundation  
The South China Sea (SCS)  
Wave flume tests  
Numerical verification  
OlaFlow

## ABSTRACT

The South China Sea (SCS) is an important channel, which plays a significant role in global economic trade and in the maintenance of world energy security. A series of artificial lands have been successfully built on the top of natural coral reefs in the SCS by the way of reclamation in recent years. In order to prevent those artificial lands from wave scouring and impacting, a great number of revetments and breakwaters have been constructed along the margin of these artificial lands. The revetment breakwaters have great significance and practical value to ensure the stability of these reclaimed lands, and to guarantee their normal long-term service performance. In this study, taking the reclamation project in the SCS as the engineering background, a computation model for the interaction between ocean waves, revetment breakwater and its calcareous coral sand foundation is established by taking the CFD solver OlaFlow as the computation platform which was developed based on the open source library OpenFOAM. Then this established computation model is verified by some laboratory testing data of wave profile and wave impact which have been measured in several wave flume physical model tests. The comparison between the testing data and the computational results indicates that the computation model established adopting OlaFlow can reliably simulate the wave generation, propagation, the dissipation of wave energy as well as the complicated interaction between ocean wave, the revetment breakwater and its calcareous coral sand foundation. This verification work will be a solid basis for the subsequent investigation of the interaction between severe ocean waves and the revetment breakwaters in large-scale, as well as the quantitative evaluation of the stability of the revetment breakwater build on reclaimed coral sand foundation in the SCS.

## 1. Introduction

The South China Sea (SCS) is rich in resources such as oil, gas, fishery, mineral deposits etc. The SCS not only acts as an important channel for global economy trade and energy transportation, but also an important strategic significance to the world economic development. Several artificial lands have been successfully built on the top of some natural coral reefs in the SCS by reclamation recently for the purpose of conducting marine observation, scientific research, maritime rescue and land protection. To defend these artificial lands from being scoured and impacted by severe waves, a great number of revetments and breakwaters have been constructed in a combined form along the margins of these reclaimed lands. However, the marine loading condition in the SCS

is relatively harsh. According to official statistics from 1949 to 1981, 366 typhoons and 198 severe typhoons have occurred in the SCS. During the past 33 years, an average of 11.1 typhoons and 6 severe ones have occurred in each year (Guan and Xie, 1984). In this case, the issue that whether the revetment breakwater is capable of withstanding the impact of severe waves or not needs to be studied comprehensively. Therefore, the investigation on the ability of the revetment breakwater when withstanding the impacting of severe ocean waves has important significance and practical value, to ensure the stability of these reclaimed lands and guarantee their long-term service performance in the SCS.

The influences of wave impacting on a breakwater can be intuitively reflected by three indicators. They are (1) the magnitude of the wave impact on breakwater; (2) the displacement of breakwater and the

\* Corresponding author.

E-mail addresses: [Yejianhongcas@gmail.com](mailto:Yejianhongcas@gmail.com), [Jhye@whrsm.ac.cn](mailto:Jhye@whrsm.ac.cn) (J. Ye).

deformation of its foundation caused by long-term wave impacting; and (3) the overtopping generated during the impacting process. Correspondingly, the stability of breakwater can be evaluated by the three indicators synthetically. At present, there have been a number of works on the hydrodynamic characteristics of the interaction between ocean waves and breakwater in literature. The wave flume physical model tests and numerical modelling are the main research methods.

At present, most of physical model tests are carried out in wave flumes due to the fact that they could simulate various ocean waves which could be similar to that occurred at the sites of practical engineering. Besides, the generated waves in wave flumes are intuitive to engineers, and with high reliability. Physical model tests in wave flume generally are conducted based on the principle of Froude number similarity under the condition of 1 g. Early tests were generally based on the assumption that seabed foundation could provide infinite bearing capacity and mainly focused their attention on the dynamics of waves and their interaction with structures. According to a great number of previous instability cases, it was found that seabed foundation actually does not have infinite bearing capacity. Instead, they were easy to become soften and/or liquefied, resulting in the losing of bearing capacity under cyclic wave impacting (Ye et al., 2015; Zhao et al., 2020). Therefore, the existence of seabed foundation has been generally taken into consideration in some wave flume tests in the past two decades (Tzang and Ou, 2006; Ulker et al., 2010; Liu et al., 2013; Shen et al., 2017; Tong et al., 2018; Yan et al., 2018; Zhang et al., 2020; Ren et al., 2020). The results obtained from these tests are more reliable for the judgment of the stability of offshore structures. Actually, a great number of experimental investigation works have been conducted through water flume tests for the hydrodynamic performance of various types of offshore breakwater in the past, such as the comparison for the effect of regular wave and random wave (Galland, 1995; Jensen et al., 1997; Günaydin and Kabdaşlı, 2007; Anastasios et al., 2019), the measurement technology for breakwater damage (Andrea et al., 2020; Jeffrey, 1999), the computation and mitigation of wave impacting (Kita et al., 2018; Mogridge and Jamieson, 1980; Franco, 1994; Oumeraci, 1994), the computation and influence factors screening for wave overtopping (Tofany et al., 2016; Salauddin and Pearson, 2019, 2020; Shankar and Jayaratne, 2003), etc. However, there also are some disadvantages such as complicated operation and high cost for the wave flume physical model tests. Therefore, it is generally only conducted for some important projects with sufficient investment.

With the rapid development of computer technology, numerical simulation has gradually become the main research method for the hydrodynamic interaction between wave and breakwater due to the advantages of simple operation and less requirement in time and laboratory space. Computational fluid dynamics (CFD) is currently the main method to simulate the hydrodynamic performance of breakwaters. The widely used CFD numerical computation methods include finite difference method (FDM), finite element method (FEM), Smoothed particle hydrodynamics (SPH) and finite volume method (FVM). The FDM is widely used in early computation models. However, the main drawback of FDM is that it is difficult to naturally deal with complex terrain and structural shape. It is also hard to achieve parallelism which leads to the limitation of computation efficiency and scale. This problem can be reflected in the program COBRAS (Hsu et al., 2002). The FEM has the advantage of high accuracy when high-order elements are used, but it also has many disadvantages, e.g., the computation meshes may need to move along with the movement of the wave. As a result, the computation efficiency could be lower while the mesh size is small, and demand for memory is huge. Therefore, the FEM is not widely used in the field of CFD, while there are still some classic works (Zienkiewicz et al., 2014; Viré et al., 2016). The SPH method has great advantages in studying

complex fluid motion like wave breaking. Additionally, its parallel efficiency is very considerable (Crespo et al., 2015). However, due to the huge amount of computation it may involve, it is quite difficult to apply the SPH method into large-scale actual marine and coastal engineering, unless the users own a cluster with GPU. Nevertheless, the FVM is currently widely used in the field of CFD due to its high parallel efficiency, relatively simple mathematical discrete theory and programming process.

As the seabed foundation is a type of porous medium, there is porous flow inside seabed foundation during the interaction between waves and structures. Unfortunately, this porous flow cannot be taken into consideration in the RANS equation. In order to solve this problem, Hsu et al. (2002) (Hsu et al., 2002) proposed the Volume Average and Reynold Average Navier Stokes (VARANS) equation which incorporates the description of pore flow into the RANS equation through the Forcheimer equation ( $I = Au + Bu^2 + c \frac{\partial u}{\partial t}$ ). OlaFlow is a solver based on the OpenFOAM open source library to solve the VARANS equation, which has been widely used in the field of coastal engineering, for example, Guler et al. (2018) (Guler et al., 2018) simulated the potential scenario of Haydarpaşa port attacked by a tsunami adopting OpenFOAM. Park et al. (2018) (Park et al., 2018) simulated and compared the three types of state for wave during the interaction between waves and structures adopting OpenFOAM and Fluent. However, the VARANS equation cannot compute the displacement of structures and the deformation of seabed foundation. In order to deal with this problem, Ye et al. (2013a), (2013b) developed an integrated model FSSI-CAS2D, which couples the VARANS equation with the Biot's equation to simulate the deformation of seabed foundation and the displacement of structure under wave impacting. Considering the safety and stability problem of the revetment breakwater built on reclaimed lands in the South China Sea under extreme wave impacting, FSSI-CAS2D will be applied into this practical engineering to carry out this type of simulation in the future. To guarantee the reliability of the computation results, it must be ensured that the VARANS equation and related solvers can accurately simulate the interaction process between the ocean wave and the revetment breakwater.

In this study, a computation model for the interaction between ocean waves, the revetment breakwater and its calcareous coral sand foundation is established based on the open source CFD solver OlaFlow. The experimental results of some wave flume physical model tests are adopted to verify the reliability of the computation model. This verification work will be a solid basis for the subsequent investigation on the stability of the revetment breakwater under severe ocean wave in the SCS.

## 2. Numerical model

### 2.1. Governing equations

The two-phase flow solver interFoam based on the RANS equation in OpenFOAM is widely applied to study the dynamics of fluids. However, the porous flow in seabed foundation can't be considered in the RANS equation. To solve this problem, Hsu et al. (2002) (Hsu et al., 2002) has proposed the VARANS equation by introducing the drag force ( $I = Au + Bu^2 + c \frac{\partial u}{\partial t}$ ) resulting from porous flow into the RANS equation. Then, the program COBRAS was developed adopting FDM. However, the structures with complex outer shape and the seabed floor with complex terrain can't be handled in COBRAS. Higuera et al. (2014) (Higuera et al., 2014) developed the computation module IHFOAM to solve the VARANS equation taking OpenFOAM as the platform, which was later evolved to OlaFlow (Higuera et al., 2018). It has overcome the shortcomings of COBRAS and it is effective to handle the interaction between

intricately shaped structures, seabed foundation with complex terrain and various ocean waves. Considering the complexity of the revetment breakwater's shape and the terrain of natural reef islands, OlaFlow is selected as the computation platform in this study. Its governing equations include the continuity equation and the momentum conservation equation:

$$\frac{\partial u_i}{\partial x_i} = 0 \quad (1)$$

$$\frac{1+c}{n} \frac{\partial \rho u_i}{\partial t} + \frac{1}{n} \frac{\partial}{\partial x_j} \left[ \frac{1}{\varphi} \rho u_i u_j \right] = -\frac{\partial (p^*)}{\partial x_i} - g_j X_j \frac{\partial \rho}{\partial x_i} + \frac{1}{n} \frac{\partial}{\partial x_j} \left[ \mu_e \frac{\partial u_i}{\partial x_j} \right] + F_i^{ST} - \alpha \frac{(1-n)^3}{n^3} \frac{\mu}{D_{50}^2} u_i - \beta \left( 1 + \frac{7.5}{KC} \right) \frac{1-n}{n^3} \frac{\rho}{D_{50}} \sqrt{u_j u_j} u_i \quad (2)$$

where,  $u_i$  is the velocity vector.  $x_i$  is the position vector.  $n$  is the porosity.  $\mu_e$  is the dynamic viscosity coefficient of water.  $\mu_e$  is the effective dynamic viscosity.  $p^*$  is the Pseudo-dynamic pressure.  $g_i$  is the acceleration due to gravity ( $g_i = 9.806 \text{ m/s}^2$ ).  $\rho$  is the density of water.

The seepage drag force formula proposed by Forchheimer (1901) (Forchheimer, 1901) and Polubarinova-Kochina (1952) (Polubarinova-Kochina, 1952) () is adopted in Equation (2) to describe the contribution of porous flow to the equation of force balance. There have been many studies on the quantitative determination of the coefficient A and B. The current widely applied formulation was proposed by Engelund (1953) (Engelund, 1953) and revised by Van Gent (1995) (Van Gent, 1995). The specific expressions are as follow:

$$A = \alpha \frac{(1-n)^3}{n^3} \frac{\mu}{D_{50}^2} \quad (3)$$

$$B = \beta \left( 1 + \frac{7.5}{KC} \right) \frac{1-n}{n^3} \frac{\rho}{D_{50}} \quad (4)$$

where  $D_{50}$  is the average particle size of porous medium.  $n$  is the porosity.  $KC$  is the Keulegan-Carpenter number, which represents the additional friction force caused by the oscillation and instability of a flowing system. It is defined as  $KC = T_0 \mu_M / D_{50} n$  where  $\mu_M$  represents the maximum oscillation rate and  $T_0$  is the oscillation period. For a steady porous flow,  $T_0$  could be set as  $+\infty$ .

$c$  in Equation (2) is a parameter related to the acceleration of porous flow. Its value is generally calculated following the equation, where is the an empirical parameter. It is proposed by Higuera et al. (2014) (Higuera et al., 2014) that  $c$  has little effect on the result. Previous researchers generally recommended the value of to be 0.34 (Higuera et al., 2014) and this value keeps unchanged in computation. It is better for  $\alpha$  and  $\beta$  to be measured by physical experiments (Ye et al., 2019) for the purpose of reliability. In addition, a series of formulations for the estimation of  $\alpha$  and  $\beta$  have been recommended by some scholars, as summarized in Lin (2007) (Lin and Karunarathna, 2007).

The VOF method is adopted in OlaFlow to capture the interface between water and air. This method introduces a phase fraction  $\alpha_{VOF}$  to represent the volume fraction of water in each grid cell. If  $\alpha_{VOF} = 1$ , it means that the mesh cell is full of water. On the contrary,  $\alpha_{VOF} = 0$  indicates that the cell is filled with air. If  $0 < \alpha_{VOF} < 1$ , it means that there is an interface between water and air, namely:

$$\begin{cases} \alpha_{VOF} = 0 & \text{Air} \\ 0 < \alpha_{VOF} < 1 & \text{Free Surface} \\ \alpha_{VOF} = 1 & \text{Water} \end{cases} \quad (5)$$

The governing equation of  $\alpha_{VOF}$  is:

**Table 1**

Reference values of the coefficients in RNG  $k-\epsilon$  model.

Coefficient	$c_\mu$	$\sigma_k$	$\sigma_\epsilon$	$C_{1\epsilon}$	$C_{2\epsilon}$	$\eta_0$	$\beta$
Value	0.0845	1.39	1.39	1.42	1.68	4.38	0.012

$$\frac{\partial \alpha_{VOF}}{\partial t} + \nabla \cdot \vec{u} \alpha_{VOF} + \nabla \cdot \vec{u}_c \alpha_{VOF} (1 - \alpha_{VOF}) \quad (6)$$

Once the phase fraction is determined, all physical parameters in each grid cell can be determined based on an average idea, for example,

the density  $\rho$  within each mesh cell is expressed as:

$$\rho = \alpha_{VOF} \rho_{water} + (1 - \alpha_{VOF}) \rho_{air} \quad (7)$$

where  $\rho_{water}$  and  $\rho_{air}$  are the density of water and air, respectively.

## 2.2. Turbulence model

There are a series of turbulence computation models available in OpenFOAM at present. The Reynolds-averaged (RANS) turbulence model is selected in this study. Generally, RANS turbulence model includes  $k-\epsilon$  model and RNG  $k-\epsilon$  model. The RNG  $k-\epsilon$  model has a better accuracy when the influence of turbulent vortices is considered. According to the work by Lu et al. (2013), the RNG  $k-\epsilon$  model can handle the flows with high strain rates and significant streamline bending more efficiently. In this study, the period of the simulated wave is small and the degree of streamline bending is relatively significant. Finally, the RNG  $k-\epsilon$  model is selected in the computation.

While the turbulence is considered in computation, it is only necessary to change  $\mu$  into  $\mu = \mu + \mu_T$  in Equation (2), where  $\mu_T$  is the eddy viscosity coefficient, formulated as

$$\mu_T = c_\mu k^2 / \epsilon \quad (8)$$

where  $k$  is turbulent kinetic energy.  $\epsilon$  is dissipation rate.  $c_\mu$  is a dimensionless constant.  $k$  and  $\epsilon$  are generally determined from the following transport equations. For the problem involving high Reynolds number, the following equations for  $k$  and  $\epsilon$  are adopted.

$$\frac{\partial k}{\partial t} + \overline{u_j} \frac{\partial k}{\partial x_j} = \frac{\partial}{\partial x_i} \left( \frac{\mu_T}{\sigma_k} \frac{\partial k}{\partial x_i} \right) + G_k - \epsilon \quad (9)$$

$$\frac{\partial \epsilon}{\partial t} + \overline{u_j} \frac{\partial \epsilon}{\partial x_j} = \frac{\partial}{\partial x_j} \left( \frac{\mu_T}{\sigma_\epsilon} \frac{\partial \epsilon}{\partial x_j} \right) + C_{1\epsilon} \frac{\epsilon}{k} G_k - C_{2\epsilon} \rho \frac{\epsilon^2}{k} \quad (10)$$

where  $G_k = 2\mu_T \overline{D_{ij} D_{ij}}$  is the turbulent kinetic energy generation term and  $D_{ij} = (\partial \overline{u_i} / \partial x_j + \partial \overline{u_j} / \partial x_i) / 2$  is the tensor of average strain rate.  $C_{1\epsilon}^* = C_{1\epsilon} - \eta(1 - \eta / \eta_0)(1 + \beta \eta^3)$ , where  $\eta = Sk / \epsilon$ ,  $S = (2\overline{D_{ij} D_{ij}})^{1/2}$ . The coefficient values in the RNG  $k-\epsilon$  model are listed in Table 1.

## 3. Physical modelling

The wave flume with a total length of 47 m, a height of 1.3 m, and a width of 1 m is adopted in the physical model tests. The left side of the flume is equipped with a piston wave maker driven by a servo motor, and there is a 7 m long inclined slope section for the purpose of wave absorption at the right end side. The revetment breakwater and its foundation are installed in the flume in the way of full section. As a

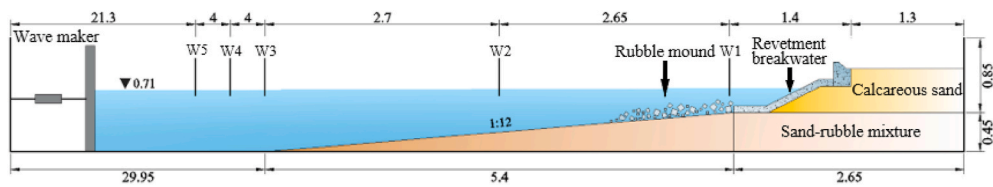


Fig. 1. Schematic map of the wave flume physical model (Unit: m).

Table 2

Physical properties of the three types of porous medium ( $I = Au + Bu^2 + c \frac{\partial u}{\partial t}$ ).

Porous Media	Average Particle Size (m)	Porosity	$\alpha$	$\beta$	
Calcareous Sand	0.0004	0.5	6.5	0.02	0.34
Sand-gravel Mixture	0.05	0.493	50	2.0	0.34
Gravels	0.012	0.5	50	0.6	0.34

Noted: A and B can be determined following Equations (3) and (4).

result, the incident waves are completely blocked and reflected by the physical model during testing. The wave absorption section actually has no use. In order to utilize the flume appropriately and let the physical model as far away from the wave maker as possible, the right end of the physical model is set at the position where is 2 m away from the starting point of the wave absorption slope. Thus, the actual effective length of the flume is 38 m in the test. The physical model is made with a geometric similarity scale of 1:10 and it is also constructed according to the real size of structures and the layout at in-site on the reclaimed coral reef islands.

The physical model designed for flume tests and its configuration are shown in Fig. 1. The revetment breakwater which is poured by concrete according to the geometric scale of 1:10 consists of a revetment and a caisson wall. The foundation of the breakwater includes three kinds of materials: gravels, sand-gravel mixture, and calcareous coral sand. Gravels and sand-gravel mixture are utilized to simulate the original stratum before the artificial land is reclaimed. The gravels simulate the coral reef flat in front of the revetment breakwater. The calcareous sand is utilized to simulate the reclaimed land on the top of natural coral reef. All the materials are sampled from the engineering in-site in the South China Sea. According to the field measurement data, the dry density of the calcareous sand foundation is  $1.51 \text{ g/cm}^3$ . The total length of the calcareous sand foundation is 2.25 m and the height is 0.5 m. The sand-gravel mixture is laid below the calcareous sand foundation with a length of 2.65 m and a height of 0.45 m. The gravels with a diameter of 1 cm–2cm is utilized to simulate the coral reef flat in front of the

breakwater for the purpose of wave energy elimination. The starting point of the coral reef flat is 29.95 m away from the wave maker. Its shape is a triangle whose length and height are 5.4 m and 0.45 m, respectively. The physical properties of three types of porous medium above determined through laboratory measurement are listed in Table 2. The measurement method for  $\alpha$  and  $\beta$  is available in Ye et al. (2019) (Ye et al., 2019).

A series of irregular rock blocks are piled up on the coral reef flat in front of the breakwater in physical testing. They are utilized to simulate the stone ripraps that is piled up in front of the breakwater to achieve the purpose of wave energy dissipation at the real engineering sites of the reclaimed coral reef islands. As demonstrated in Fig. 1, the average diameter of the rock blocks is about 10 cm, and their installment length is about 1 m. In order to further enhance the wave dissipation ability at the engineering sites, a series of accropodes are installed on the revetment breakwater in a staggered way. In the wave flume physical model tests, a great number of accropodes are also installed in the same way in front of the revetment breakwater, as shown in Fig. 2 (b). The length,

Table 3

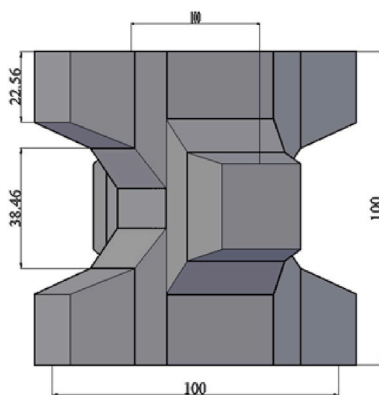
Positions of the wave profile gauges (The left side of the flume is taken as the reference point).

Wave Profile Gauges Number	Distance (m)
W1	2.7
W2	5.35
W3	8.05
W4	12.05
W5	16.05

Table 4

Experimental conditions in the wave flume physical model tests.

Test No.	Water Depth (m)	Period (s)	Wave Height (m)	Accropodes
1	0.48 (Low)	1.7	0.23	No
2	0.71 (High)	2.2	0.3	No
3	0.71 (High)	2.2	0.3	Yes



(a) Single accropode



(b) Staggered installment

Fig. 2. A real view of the staggered installment of accropodes in front of the revetment breakwater.

**Table 5**  
Experimental wave conditions in the model verification tests without structure.

Test No.	Water Depth (m)	Period (s)	Wave Height (m)
A	0.48	1.7	0.1
B	0.48	1.7	0.15
C	0.48	1.7	0.2
D	0.71	2.2	0.1
E	0.71	2.2	0.2
F	0.8	2.2	0.1
G	0.8	2.2	0.2

width and height of accropode model are all 0.1 m, as demonstrated in Fig. 2 (a).

In the wave flume physical model tests, thirty-two pressure sensors are installed on the revetment and caisson to record the impact pressure of wave on the revetment breakwater. Five wave profile gauges are installed along the longitudinal central line of the flume to record the variation of water level in tests. The positions of the five wave profile gauges are shown in Fig. 1. According to the distance to the breakwater, the wave profile gauges are numbered W1 to W5 from far to near position. The distance of the wave profile gauges from the rightmost end of the physical model are listed in Table 3.

Considering different water levels, wave heights and periods, more than 10 tests have been conducted. In this study, the test results of three typical wave conditions are selected to verify the reliability of the established computation model. The wave parameters listed in Table 4 are the target parameters of the generated regular waves, which is generated by a piston wave maker.

**4. Model verification without structure**

In order to build a foundation for the verification of the subsequent

complex cases, it is necessary to verify the numerical computation model adopting the results obtained in some simple water flume tests. In this study, totally 7 sets of wave flume tests without any structures have been conducted for this purpose. The wave parameters of them are listed in Table 5. It is noticed that the wave parameters listed in Table 5 also are the target waves, and the Stokes wave theory of second-order is adopted by the numerical wave maker. The wave profile recorded by W3 is adopted to verify the numerical computation model.

The comparison between the test results recorded by W3 and the computational results of the numerical model under the 7 sets of experimental wave conditions is illustrated in Fig. 3. It is observed in Fig. 3 that the numerical computation model can accurately generate the waves required in the tests. Since the physical wave maker just started to work in the initial 10s, the entire wave-making system is a little unstable during this period. As a result, the agreement between the numerical simulation results and the experimental results is relatively poor in the initial 10s. However, the physical wave maker became stable to work after  $t = 10s$ , the numerical results can agree very well with the test results, as demonstrated in Fig. 3.

Through the comparative analysis, it is indicated that the wave maker in OlaFlow can reliably simulate various simple water waves. Furthermore, there is no the requirement for OlaFlow that a period of time is necessary for the wave profiles become stable, like that in the physical model tests. After OlaFlow starting to generate wave, the wave height can steadily reach its expected value in short period. Finally, the phenomenon of wave height attenuation and wave interference are both not observed in the numerical wave flume. It is indicated that OlaFlow has efficiently and successfully absorbed the incident wave at the end boundary of numerical wave tank by setting the active wave absorption boundary condition.

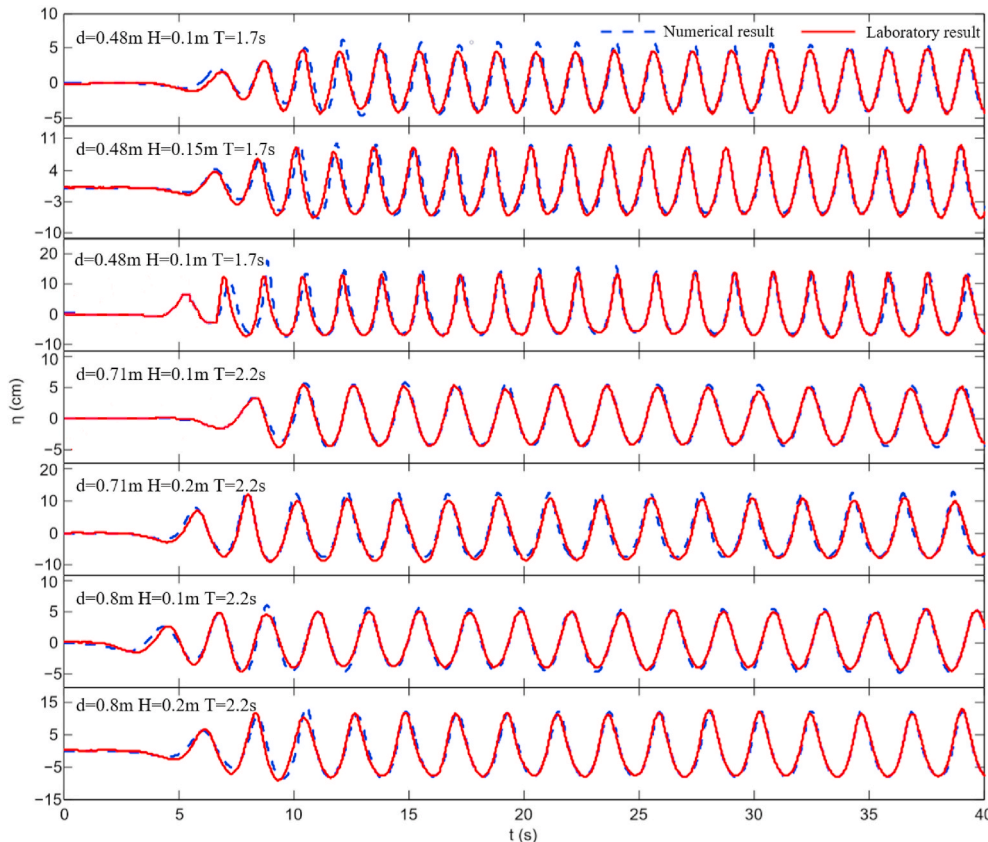


**Fig. 3.** Comparison of the wave profiles at the position of W3 between the numerical and the physical model test results in the cases without structure.

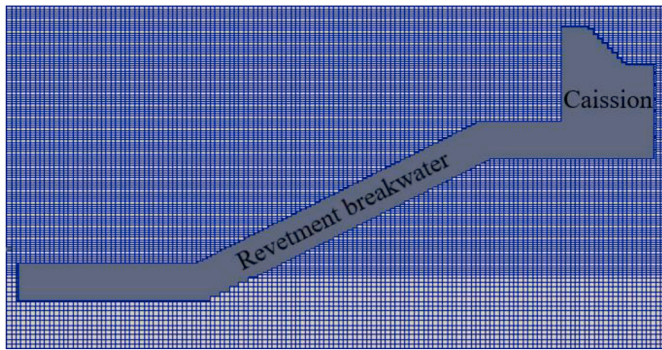


Fig. 4. Schematic map of the mesh around the revetment breakwater (without accropode).

**5. Model verification for wave-revetment breakwater-calcareous coral foundation interaction**

Although the numerical wave maker of OlaFlow has been tested in the cases without structures, whether the computational model established based on OlaFlow for the wave-revetment breakwater-calcareous coral sand foundation interaction could reliably simulates the complicated interaction process still requires further verification. The results obtained from the three physical model tests listed in Table 4 are adopted to verify the established computational model in this section.

In order to perform the numerical simulation efficiently, a super cluster Huawei KunLun9016 is utilized. There are totally 256 CPU cores have been used in parallelization. The CPU type is Intel Xeon E7-4850 v4 and its frequency is 2.10 GHz. The memory demand for Tests 1 to Test 3 are 3.2 GB, 3.9 GB and 11.7 GB. There are 370806, 547579 and 4171577 elements in Test 1, Test2 and Test 3, respectively. For each case presented in this section, the time spend for computation are 6.4 h for Test 1, 7.5 h for Test 2 and 115.6 h for Test 3, respectively.

**5.1. Mesh generation**

In order to simulate the wave propagation process and the interaction between the wave and the structure effectively, non-uniform mesh system is used during the mesh generation in the established numerical model. As it is shown in Fig. 4, the meshes near to the water-air interface and around the structure are relatively dense, while they are relatively loose in the other zone.

The revetment breakwater is not meshed as it is impervious concrete material. The foundation of the revetment breakwater is porous medium. Thus, it needs to be meshed considering the internal porous flow in it.

As listed in Table 4, accropodes are utilized to dissipate the wave energy in Test 3. The number of meshes will be very great (probably up to hundreds of millions), if the meshes around the accropodes are generated based on the configuration in the physical model tests. Furthermore, it is quite difficult to perform the mesh generation operation as these accropodes are mutually contacted with each other. Therefore, in order to simplify the computation and improve the

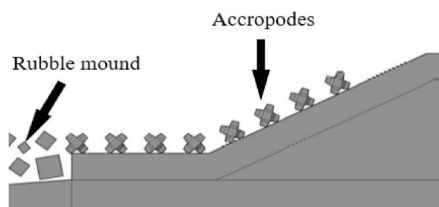


Fig. 5. Configuration of these accropodes and the rubble mound in the computation model.

computation efficiency, the accropodes in the computation model are installed in the way shown in Fig. 5. Only one row of accropodes is placed on the revetment breakwater.

In the cases without accropodes, only two-dimensional mesh is required. Nevertheless, for those cases with accropodes, three-

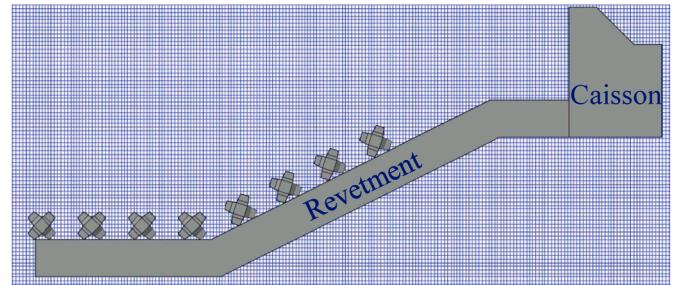


Fig. 6. Generated meshes around the revetment breakwater and these accropodes in the computation model for Test 3.

**Table 6**

Mesh sizes of computational cells for Test 1 (low water level).

Direction	Region (m)	Cell Number	Size (cm)
X	0–15	1500	1
	15–24	900	1
	24–25	100	1
Z	0–0.32	32	1
	0.32–0.62	60	0.5
	0.62–1.2	58	1

**Table 7**

Mesh sizes of computational cells for Test 2 (high water level).

Direction	Region (m)	Cell Number	Size (cm)
X	0–15	750	2
	15–24	900	1
	24–25	20	5
Z	0–0.5	50	1
	0.5–1.8	260	0.5
	1.8–2	20	1

**Table 8**

3D mesh sizes of computational cells for Test 3 (high water level).

Direction	Region (m)	Cell Number	Size (cm)
X	0–15	750	2
	15–24	900	1
	24–25	20	5
Y	0–0.1	10	1
Z	0–0.5	50	1
	0.5–1.8	260	0.5
	1.8–2	20	1

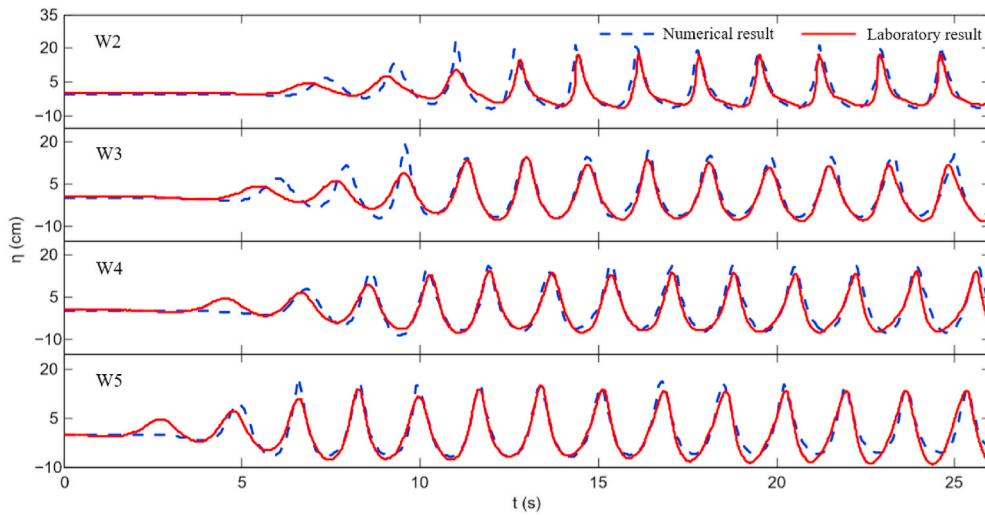


Fig. 7. Comparison of the wave profiles between the numerical results and the water flume testing data in Test 1 (low water level without accropodes).

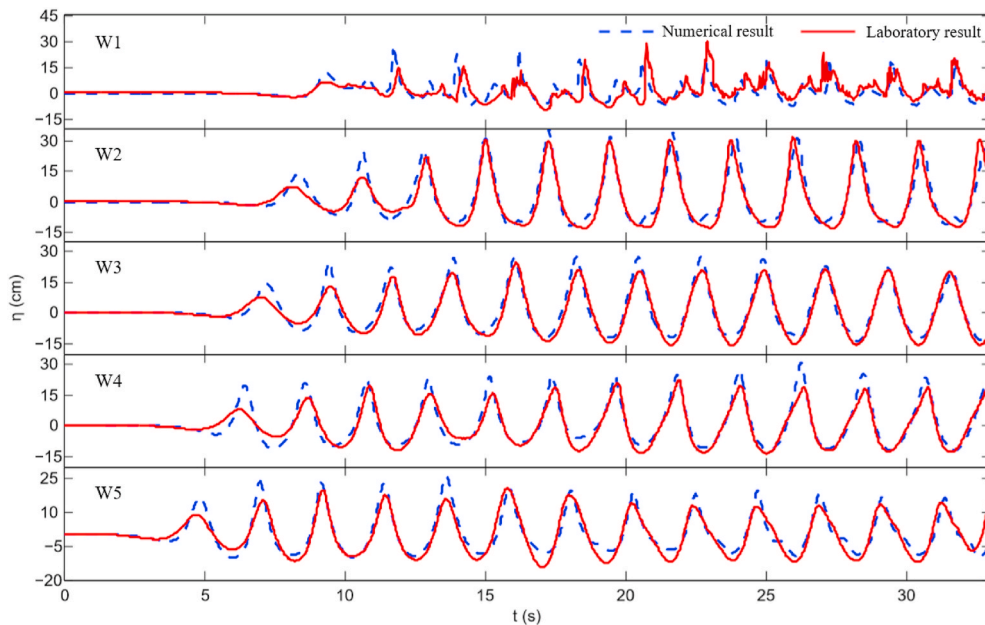


Fig. 8. Comparison of the wave profiles between the numerical results and the test results recorded in Test 2 (high water level without accropode).

dimensional meshes must be generated. The mesh generation is performed adopting the meshing tool (Utilities) available in the OpenFoam library. The generated meshes in the case with accropodes are shown in Fig. 6. The detailed information about the mesh size of the computational cells for Test 1, Test 2 and Test 3 are listed in Tables 6–8.

### 5.2. Comparative analysis for wave surfaces

The comparison for the wave profiles between the numerical results and the test results recorded in Test 1 (low water level without accropode) is illustrated in Fig. 7. W4 and W5 are located in the middle part of the wave flume, which mainly are utilized to measure the ability of wave maker. The wave profiles at W4 and W5 reach the expected wave height at the time of 10s and 8s, respectively, and maintain a good stability thereafter. W2 is located over the zone of the triangular coral reef flat. W3 is located at the beginning of the reef flat. The wave profiles recorded by them are basically the same as that recorded by W4 and W5. However, the wave profile at W2 is a little different due to the effect of

the wave climbing on the sloping reef flat. At the same time, the wave crests become significantly sharper and the wave troughs get a little flatter, showing obvious nonlinearity. Due to the shallow water depth in Test 1, and W1 is located in front of the revetment, there is no wave profile that can be recorded because no wave has arrived at there.

It is demonstrated in Fig. 7 that the computation results of the numerical model are in good agreement with the physical model tests results under the low water level without accropodes. It is indicated that the numerical computation model has good reliability.

The comparison of the wave profiles between the numerical model results and the test results recorded in Test 2 (high water level without accropodes) is demonstrated in Fig. 8. It is shown by the wave profile at W1 that the period between two main crests maintains about 2.2s. Additionally, there are a series of secondary crests between two main crests. The reason for this phenomenon is that W1 is located above the rubble mounds in front of the revetment. Significant reflection and superposition with the incident waves and wave breaking always occur at the position of W1, which certainly lead to a very irregular wave profile

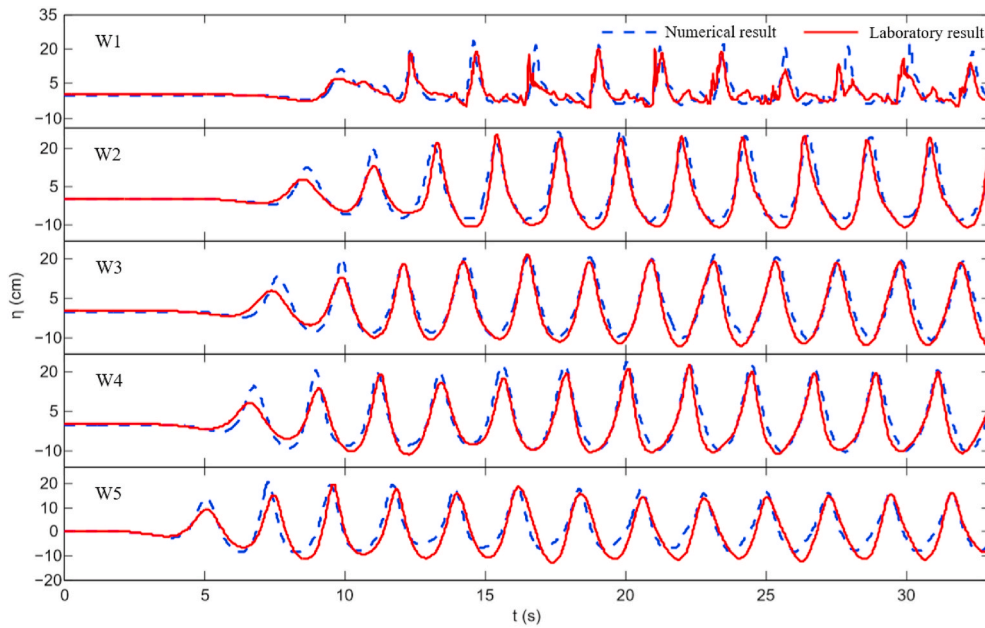


Fig. 9. Comparison of the wave profiles between the numerical results and the test results recorded in Test 3 (high water level with accropodes).

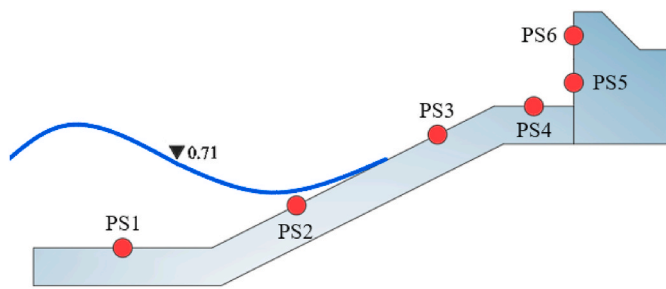


Fig. 10. Position of the pressure sensors installed on the revetment breakwater (PS means pressure sensor).

at W1. As a consequence of the high water level in Test 2, the climbing effect of the wave at W2 is not particularly significant. However, there is still the phenomenon that the wave crests become sharper and the troughs get flatter. At the same time, the wave height at this position W2 has the trend of increasing which can reach about 40 cm.

As shown in Fig. 8, the computed wave profiles at W2 to W5 are basically consistent with the testing data from the physical model test for the case with high water level and without accropode. W1 is located at the left end of the revetment and meanwhile at the right end of the rubble mound. Due to the wave reflection, superposition and the energy

dissipation of the rubble mounds, the evolution of the wave profile at W1 is very complicated. Although the influence of the rubble mound is considered in the computation model, and only one row of accropodes are set, this is quite different from the real installment of the accropodes in the physical model. Therefore, it is normal that there are some differences between the computed wave profiles and the testing results at the position W1. But it still can be seen in Fig. 8 that the computed and recorded wave profiles are quite similar. It is indicated that the established numerical calculation model is credible.

The comparison of wave profiles between the numerical model results and the test results in Test 3 (high water level with accropodes) is demonstrated in Fig. 9. Generally, compared with that in Test 2, the wave profile at W1 is more regular since the wave energy is dissipated by the accropodes. The retreating of waves from the revetment breakwater has little effect on the incident wave. As a result, the reflected wave does not cause much interference to the next incident wave after the wave breaking and hitting the breakwater in each period. Finally, only a little fluctuation appears at each trough.

Even though the mesh is relatively more complicated after the accropodes are added in the numerical computation model, OlaFlow can still handle the simulation of wave generation, wave breaking and porous flow very well. The simulation result at W1 with a crest height of 20 cm is more stable than that of experimental data. It happens due to the following several factors. Firstly, the number of accropodes has been

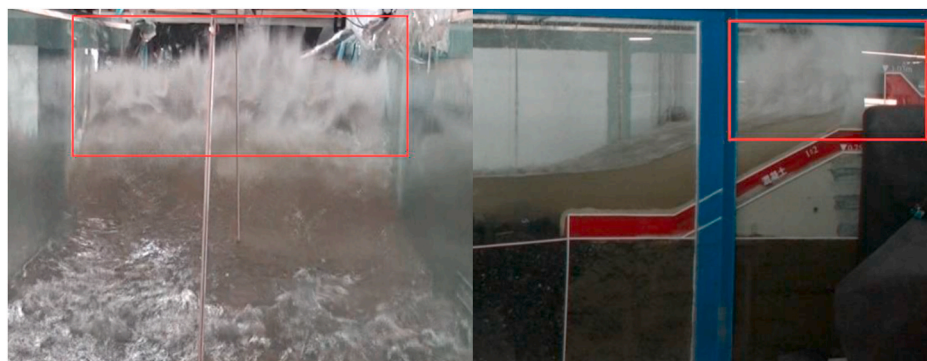


Fig. 11. Wave breaking, overtopping and wave impacting on the caisson wall.

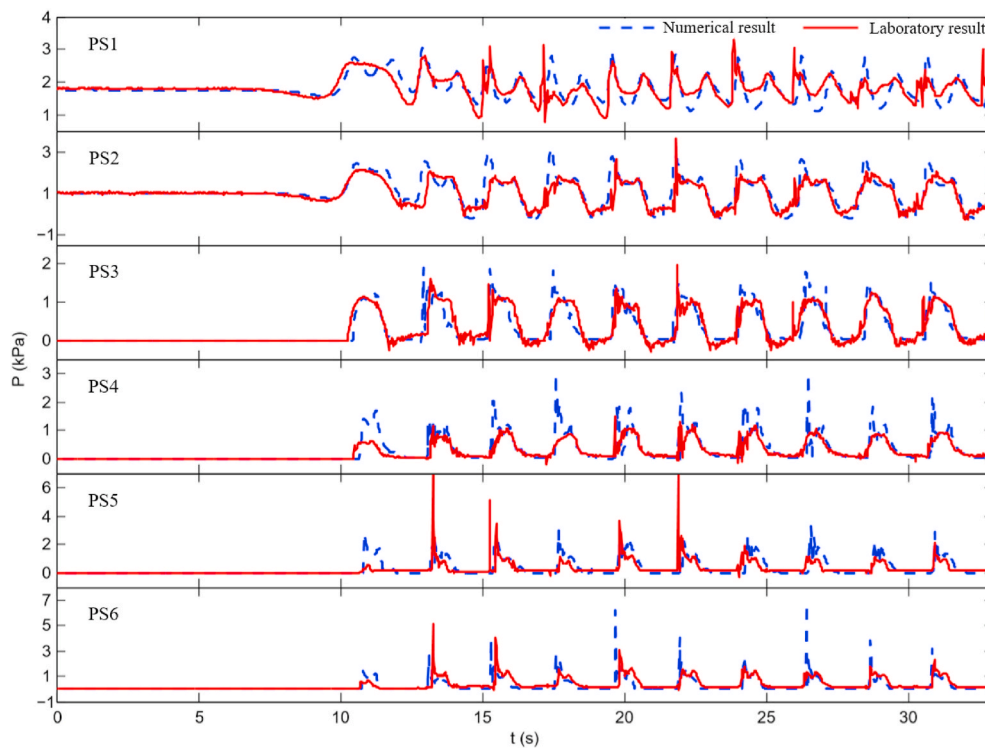


Fig. 12. Time history comparison of the wave impact between the numerical simulation results and the test results in Test 2 (high water level without accropode).

greatly reduced comparing with that in the physical model tests; and the installment way also has been simplified. Secondly, the width of the flume is reduced and the surface roughness is out of consideration. That is to say, the simulation environment in the computation model is relatively simple and ideal. In general, the computational results of wave profile at W1 are basically consistent with the testing results. The simulated results at W2 to W5 also fit well with the testing results.

Therefore, in the case of high water level with accropodes, the established numerical computation model in this study also has good reliability.

### 5.3. Comparative analysis of wave impact pressure

In the physical model tests, thirty two pressure sensors are uniformly

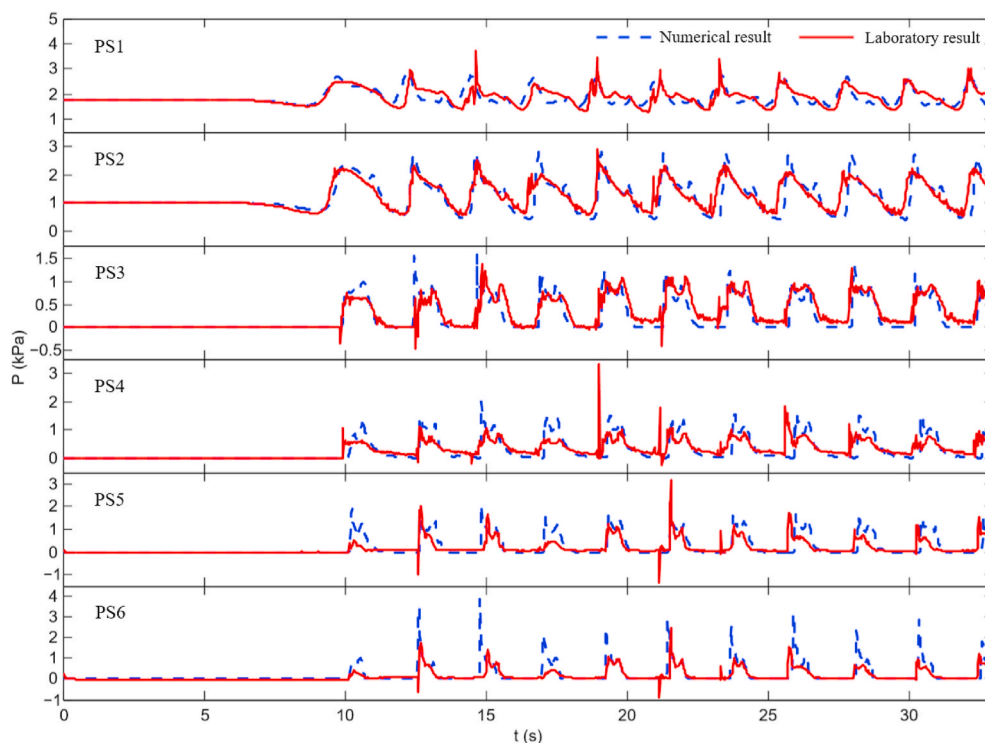


Fig. 13. Time history comparison of the wave impact between the numerical simulation results and test results in Test 3 (High water level with accropodes).

installed on the revetment breakwater to record the impact of wave. Six pressure sensors named PS1 to PS6 at typical positions are taken as the representative to verify the computation model. The specific position and serial number of the six pressure sensors are shown in Fig. 10. The outer diameter of the pressure sensors is 5 mm. The measuring range is 10 kPa with a measuring accuracy of 0.25%. The sampling frequency is 50 Hz during testing.

As the water level is low in Test 1, the revetment breakwater is not attacked by the waves. Therefore, the comparative analysis of the impact pressure is not studied for Test 1.

The time history comparison of the wave impact between the numerical simulation results and the test results at the six typical positions on the revetment breakwater in Test 2 (High water level without accropodes) is shown in Fig. 12. Except for that recorded by PS1, the wave impact recorded by the other five pressure sensors all show a good periodicity. PS1 is located at the left end of the revetment, where the incident wave and reflected wave are superimposed violently. The wave profile is greatly affected by the superposition, so the time history of wave impact has great fluctuation. PS2 and PS3 are located on the slope of the revetment. The wave impact recorded by PS2 and PS3 are quite similar. Besides, there are a great number of high-frequency fluctuations on the crest and trough zones in the time history of wave impact. PS4 is located at the right end of the revetment. The time history of wave impact recorded by PS4 is basically the same as that recorded by PS2 and PS3. PS5 and PS6 are installed on the lateral side of the caisson wall to directly record the time-history of wave impact on it. It can be found that there is no obvious wave breaking on the slope of the revetment when the incident wave crests reaching the revetment breakwater. However, the wave crests climb along the sloping upper surface of the revetment and finally impact the lateral side of the caisson wall fiercely, resulting in the severe breaking and wave overtopping as that shown in Fig. 11.

The wave impact on the caisson wall recorded by PS5 and PS6 have the typical characteristics of impacting. The impact of wave reaches its peak value which is up to 5 kPa in a short time when the wave is colliding with the caisson wall. Then the wave impact quickly reduces to the magnitude of 1/2 to 1/3 of the peak value, and maintains for a period of time. It finally reduces rapidly after the wave retreating, but it does not completely reduce to 0, because there is more or less water accumulated in the holes where the pressure sensors are installed.

It is a fact that the shape and the random layout of these rubbles in front of the revetment can't be exactly simulated in computation. Moreover, the surfaces of the reef flat and the revetment breakwater are smooth in the numerical modelling. However, they are actually rough in the physical model tests. As a result, the wave impact predicted by the numerical simulation is slightly greater than the testing value at each position. The agreement on the time history of wave impact at PS1 between the numerical result and the recorded value in testing is not very well, because the wave characteristics at PS1 is greatly affected by the rubbles in the physical model tests. However, it is difficult for the numerical model to handle this effect accurately. It should be noticed that the numerical results are just slightly different with the testing results such as the peak impact pressure and the wave period. Besides, the numerical model is successful in capturing the secondary peak value of the wave impact which is caused by the wave retreating. This secondary peak value of the wave impact pressure is basically consistent with the wave profiles recorded in the physical model tests. The computation results of the wave impact at PS2 and PS3 are as same as the results recorded in the physical tests. What is quite different from the physical test results is that the impacting and retreating of the wave are relatively smooth in the numerical simulated results. Additionally, there is no the high-frequency fluctuation in the crest and trough zones along the time history of the wave impact predicted by the computational model, because the surface of the revetment breakwater is approximately smooth in the geometry model for numerical modelling. The time history characteristics of the wave impact on the caisson wall at PS5 and PS6 are also well simulated by the numerical model. The comparison of

the wave impact between the time-history and the numerical simulation results is shown in Fig. 12. It is observed that the computation model can reliably determine the magnitude and the time-history of the wave impact acting on the revetment breakwater under the condition of high water level without accropode.

The time history comparison of the wave impact between the numerical simulation results and the test results in Test 3 at the six typical positions on the revetment breakwater (high water level with accropodes) are illustrated in Fig. 13. After these accropodes are installed, the time history of the wave impact at the six positions all showcase a good periodicity. It is quite different from that in Test 2 as shown in Fig. 12. Since these accropodes can effectively dissipate some wave energy, there is no significant wave superposition and wave breaking at PS1. Comparing with that in Test 2, the time history of the wave impact at PS1 has a better periodicity and there is no obvious secondary peak. The time history of the wave impact recorded by PS5 and PS6 on the caisson wall indicates that the energy dissipation effect of these accropodes is effective and considerable. The peak of the wave impact is only about 2 kPa, which is reduced by 60% relative to that in Test 2.

It is demonstrated in Fig. 13 that the computational results of the numerical model and the testing results recorded in the physical model tests are in good consistency. It is indicated that the established numerical computational model has good reliability under the conditions of high water level with accropodes.

Through the comparative analysis between the numerical results and the physical model tests results, it is found that the numerical computational model established in this study for the interaction between ocean waves, revetment breakwater and its calcareous coral sand foundation can reliably simulate the wave propagation, reflection, superposition, breaking, overtopping and the physical process of wave impacting on the revetment breakwater. It will be a solid basis for the subsequent investigation of the dynamics characteristics of the revetment breakwater and the deformation of its calcareous coral foundation, as well as the evaluation of stability of the revetment breakwater in the SCS.

## 6. Conclusion

Taking the reclamation project in the SCS as the engineering background, a numerical computational model for Wave-Revetment breakwater-Calcareous coral sand foundation Interaction is established in this study taking the open source CFD solver *OlafFlow* as the computational platform. A series of physical model tests are also conducted in a large wave flume adopting a geometric scale of 1:10. Through the comparative analysis on the wave profiles and the time history of the wave impact acting on the revetment breakwater between the numerical results and the testing results, it is found that the numerical computational model established for the interaction between ocean waves, revetment breakwater and its coral sand foundation has good reliability. This numerical verification work will be a solid basis not only for the subsequent investigation on the interaction between extreme ocean waves, revetment breakwaters in the SCS and their coral sand foundation at the practical engineering scale, but also for the quantitative evaluation of the stability of the revetment breakwater in extreme typhoon climate in the SCS.

## CRediT authorship contribution statement

**Jianhong Ye:** Conceptualization, Methodology, Writing – review & editing, Supervision, Project administration, Funding acquisition. **Jipeng Shan:** Investigation, Formal analysis, Validation. **Haoran Zhou:** Writing – original draft, Writing – review & editing. **Naixiao Yan:** Visualization, Writing – original draft.

## Declaration of competing interest

The authors declare that they have no known competing financial interests or personal relationships that could have appeared to influence the work reported in this paper.

## Acknowledgement

This work is grateful for the funding support from National Natural Science Foundation of China, Grant No. 51879257, as well as the funding support from “Strategic Priority Research Program of the Chinese Academy of Sciences”, Grant No. XDA13010202.

## References

- Anastasios, S.M., Georgios, Th.K., Constantine, D.M., Athanassios, A.D., 2019. Hydrodynamic conditions in a submerged porous breakwater. *Ocean Eng.* 172, 712–725.
- Andrea, M., Tiago, C.A.O., Agustin, S.A., Xavier, G., 2020. Effect of wave storm representation on damage measurements of breakwaters. *Ocean Eng.* 200, 107082.
- Crespo, A.J.C., Domínguez, J.M., Rogers, B.D., Gómez-Gesteira, Longshaw, M.S., Canelas, R., Vacondio, R., Barreiro, A., García-Feal, O., 2015. DualSPHysics: open-source parallel CFD solver based on smoothed particle hydrodynamics (SPH). *Comput. Phys. Commun.* 187, 204–216.
- Engelund, F., 1953. On the laminar and turbulent flow of ground water through homogeneous sand. *Trans. Danish Acad. Tech. Sci.* 3.
- Forchheimer, P., 1901. Wasserbewegung durch Boden. *Z. Ver. Deutsch. Ing.* 45, 1782–1788.
- Franco, L., 1994. Vertical breakwaters: the Italian experience. *Coast. Eng.* 22 (1–2), 31–55.
- Galland, J.C., 1995. Rubble mound breakwater stability under oblique waves: an experimental study. In: 25th International Conference on Coastal Engineering. ASCE, pp. 1061–1074.
- Guan, F.C., Xie, Q.H., 1984. Statistical characteristics of South China Sea typhoon. *Mar. Sci. Bull.* 4, 21–29.
- Guler, H.G., Baykal, C., Arikawa, T., Yalciner, A.C., 2018. Numerical assessment of tsunami attack on a rubble mound breakwater using openfoam. *Appl. Ocean Res.* 72, 76–91.
- Günaydin, K., Kabdaşlı, M.S., 2007. Investigation of Pi-type breakwaters performance under regular and irregular waves. *Ocean Eng.* 34 (7), 1028–1043.
- Higuera, P., Lara, J.L., Losada, I.J., 2014. Three-dimensional interaction of waves and porous coastal structures using OpenFOAM. Part I: formulation and validation. *Coast. Eng.* 83 (1), 243–258.
- Higuera, P., Liu, P., Lin, C., Wong, W., Kao, M., 2018. Laboratory-scale swash flows generated by a non-breaking solitary wave on a steep slope. *J. Fluid Mech.* 847, 186–227.
- Hsu, T.J., Sakakiyama, T., Liu, L.F., 2002. A numerical model for wave motions and turbulence flows in front of a composite breakwater. *Coast. Eng.* 46 (1), 25–50.
- Jeffrey, A. Melby, 1999. Damage progression on Rubble-Mound breakwaters. *Coast. Eng.* 1998, 1884–1897.
- Jensen, T., Andersen, H., Grønbech, J., Mansard, E.P.D., Davies, M.H., 1997. Breakwater stability under regular and irregular wave attack. In: 25th International Conference on Coastal Engineering. ASCE, pp. 1679–1692.
- Kita, Tsukasa, Suzuki, Kojiro, Tsuruta, Naoki, Burgess, Kevin, January 2018. Experimental study on breakwater against overflow and big waves. In: Proceeding of Coasts, Marine Structures and Breakwaters 2017, pp. 1141–1149.
- Lin, P., Karunaratna, S.A.S.A., 2007. Numerical study of solitary wave interaction with porous breakwaters. *J. Waterway Port Coast. Ocean Eng., ASCE* 133 (5), 352–363.
- Liu, X., Jia, Y., Zheng, J., Hou, W., Zhang, L., Zhang, L., Shan, H., 2013. Experimental evidence of wave-induced inhomogeneity in the strength of silty seabed sediments: Yellow River Delta, China. *Ocean Eng.* 120–128.
- Lu, K., Qi, L.M., Wang, X., Han, L.S., Wang, H.M., 2013. Application and comparison of different turbulence model in the simulation of numerical wave flume. *Mar. Sci. Bull.* 32 (6), 695–699.
- Mogridge, G.R., Jamieson, W.W., 1980. Wave impact pressures on composite breakwaters. In: 25th International Conference on Coastal Engineering. ASCE, pp. 1829–1848.
- Oumeraci, H., 1994. Review and analysis of vertical breakwater failures – lessons learned. *Coast. Eng.* 22 (1–2), 3–29.
- Park, H., Do, T., Tomiczek, T., Cox, D.T., Van, D.L.J.W., 2018. Numerical modeling of non-breaking, impulsive breaking, and broken wave interaction with elevated coastal structures: laboratory validation and inter-model comparisons. *Ocean Eng.* 158, 78–98.
- Polubarinova-Kocina, 1952. Theory of Motion of Ground Water. Gosudarstv. Izdat. Tehn. Teor. Lit, Moscow.
- Ren, Y.P., Xu, G.H., Xu, X.B., Zhao, T.L., Wang, X.Z., 2020. The initial wave induced failure of silty seabed: liquefaction or shear failure. *Ocean Eng.* 200, 106990.
- Salaudinn, M., Pearson, J.M., 2019. Wave overtopping and toe scouring at a plain vertical seawall with shingle foreshore: a physical model study. *Ocean Eng.* 171, 286–299.
- Salaudinn, M., Pearson, J.M., 2020. Laboratory investigation of overtopping at a sloping structure with permeable shingle foreshore. *Ocean Eng.* 197, 106866.
- Shankar, N.J., Jayaratne, M.P.R., 2003. Wave run-up and overtopping on smooth and rough slopes of coastal structures. *Ocean Eng.* 30 (2), 221–238.
- Shen, J.H., Wu, H.C., Zhang, Y.T., 2017. Subsidence estimation of breakwater built on loosely deposited sandy seabed foundation: elastic model or elasto-plastic model. *Int. J. Naval Arch. Ocean Eng.* 9 (4), 418–428.
- Tofani, N., Ahmad, M.F., Mamat, M., Mohd-Lokman, H., 2016. The effects of wave activity on overtopping and scouring on a vertical breakwater. *Ocean Eng.* 116, 295–311.
- Tong, L., Zhang, J., Sun, K., Guo, Y., Zheng, J., Jeng, D., 2018. Experimental study on soil response and wave attenuation in a silt bed. *Ocean Eng.* 105–118.
- Tzang, S., Ou, S., 2006. Laboratory flume studies on monochromatic wave–fine sandy bed interactions Part 1. Soil fluidization. *Coast. Eng.* 53 (11), 965–982.
- Ulker, M.B., Rahman, M.S., Guddati, M.N., 2010. Wave-induced dynamic response and instability of seabed around caisson breakwater. *Ocean Eng.* 37 (17), 1522–1545.
- Van Gent, M.R.A., 1995. Wave Interaction of Permeable Coastal Structures. Ph.D. thesis. Delft University, Delft, The Netherlands.
- Viré, A., Spinneken, J., Piggott, P., Pain, C.C., Kramer, S CEur, 2016. Application of the immersed-body method to simulate wave–structure interactions. *J. Mech. B. Fluids* 55 (2), 330–339.
- Yan, Z., Zhang, H.Q., Sun, X.P., 2018. Tests on wave-induced dynamic response and instability of silty clay seabeds around a semi-circular breakwater. *Appl. Ocean Res.* 1–13.
- Ye, J., Jeng, D.S., Wang, R., Zhu, C.Q., 2013a. Validation of a 2-D semi-coupled numerical model for fluid–structure–seabed interaction. *J. Fluid Struct.* 42, 333–357.
- Ye, J., Jeng, D.S., Wang, R., Zhu, C.Q., 2013b. A 3D semi-coupled numerical model for fluid–structures–seabed–interaction (FSSI-CAS 3D): model and verification. *J. Fluid Struct.* 40, 148–162.
- Ye, J., Jeng, D., Ren, W., Changqi, Z., 2015. Numerical simulation of the wave-induced dynamic response of poro-elastoplastic seabed foundations and a composite breakwater. *Appl. Math. Model.* 39 (1), 322–347.
- Ye, J.H., Zhang, Z.H., Shan, J.P., 2019. Statistics-based method for determination of drag coefficient for nonlinear porous flow in calcareous sand soil. *Bull. Eng. Geol. Environ.* 78 (5), 3663–3670.
- Zhang, Q., Zhai, H., Wang, P., Wang, S., Jeng, D.S., 2020. Experimental study on irregular wave-induced pore-water pressures in a porous seabed around a mono-pile. *Appl. Ocean Res.* 95, 102041.
- Zhao, H.Y., Zhu, J.F., Liu, X.L., Jeng, D.S., Zhang, J.S., 2020. Numerical investigation of dynamic soil response around a submerged rubble mound breakwater: ii. loose sandy seabed. *Ocean Eng.* 215, 107891.
- Zienkiewicz, O.C., Taylor, R.L., Nithiarasu, P., 2014. The Finite Element Method for Fluid Dynamics, seventh ed. Butterworth-Heinemann, Elsevier.